scientific reports

Check for updates

OPEN

Biocompatible autonomous self-healing PVA-CS/TA hydrogels based on hydrogen bonding and electrostatic interaction

Xiaogang Yu[1,3], Jinxin Huang[2,3], Chengwei Wu[2] & Wei Zhang[2]✉

The biocompatible autonomous self-healing hydrogels have great potential in biomedical applications. However, the fairly weak tensile strength of the hydrogels seriously hinders their application. Here, we introduced chitosan (CS) into the polyvinyl alcohol (PVA)-tannic acid (TA) hydrogel and investigated the effects of the CS content, as CS can not only form reversible H bonds with PVA and TA but also form reversible electrostatic interactions with TA. Since the bond energy of electrostatic interaction is much stronger than that of the H bond, the tensile strength and self-healing properties of PVA-TA hydrogel can potentially be improved by adding the CS. The results suggested that when the PVA content and the total content of CS and TA were fixed (PVA: 30 wt.%; CS + TA: 3 wt.%) and the CS content was increased to 1 wt.%, the tensile strength of the PVA-CS/TA hydrogel could be up to 447 kPa, and the self-healing efficiency remained at 84% in 2 h. Compared with the reported self-healing hydrogels with similar biocompatibility and self-healing properties, whose tensile strength is usually less than 300 kPa, the PVA-CS/TA hydrogel prepared here shows a significant improvement in the tensile strength.

Keywords Self-healing hydrogel, Mechanical strength, Biocompatibility

Hydrogel is a gel with a hydrophilic 3D polymer network structure formed by physical or chemical cross-linking, which has a broad application in the biomedical field[1]. For example, the biomimetic hydrogel with a porous structure is conducive to the transmission of nutrients and oxygen and can be used to imitate the highly hydrated extracellular matrix due to its high water content (50–90%), which is conducive to cell culture[2]. However, due to the effect of dynamic loads on the human body, the biomedical hydrogels acting on the human body are usually easily damaged, resulting in the failure of the hydrogel function, which brings certain hidden dangers to the life safety of the patients[3]. Thus, a high mechanical strength is usually required for biomedical hydrogel to extend its service life as much as possible. On other hand, if the biomedical hydrogel possesses good self-healing properties can quickly and automatically heal some minor damages, the service life of the biomedical hydrogel can also be effectively extended. Based on this, a lot of research work has been carried out on self-healing hydrogels. At present, self-healing hydrogels have shown great application potential in biomedical fields such as tissue engineering, cell/drug delivery, and biological tissue replacement materials[4,5].

Although some progress has been made on developing self-healing hydrogels, their weak mechanical strength, severe self-healing conditions, and poor biocompatibility still limit their application in biomedicine. The hydrogels for bearing use are always designed with adequate mechanical strength to sustain physical loads. However, the reported high-strength hydrogels usually showed unsatisfactory self-healing performance. Li et al.[6] utilized the reversible reconstruction of hydrogen bonds and ionic bonds to develop the self-healing Agar/PAAc-Fe^{3+} double network hydrogel. The obtained tensile strength has reached 820 kPa, but it could recover only 27.5% after 48 h of self-healing. Liu et al.[7] prepared a self-healing composite hydrogel containing graphene oxide (GO) with a tensile strength of 350 kPa. After self-healing at 30 °C for 72 h, the self-healing rate was only 42%. Zhang et al.[8] developed a physically cross-linked PVA hydrogel with a tensile strength of up to 200 kPa. But the self-healing process was slow, with strength restored to 72% after 48 h. In order to improve the self-healing properties of high-strength hydrogels, researchers are trying to use external stimuli as self-healing

[1]Xinyu Key Laboratory of Materials Technology and Application for Intelligent Manufacturing, School of Mechanical and Electrical Engineering, Xinyu University, Xinyu 338004, China. [2]State Key Laboratory of Structure Analysis, Optimization and CAE Software for Industrial Equipment, Department of Engineering Mechanics, Dalian University of Technology, Dalian 116024, China. [3]Xiaogang Yu and Jinxin Huang contributed equally to this work. ✉email: wei.zhang@dlut.edu.cn

conditions (high temperature, magnetic field, light irradiation, etc.) to improve the self-healing properties of hydrogels. Whereas, this not only adds complexity to the self-healing process but also restricts the application scenarios in biomedicine[9–13]. In addition, developing high-strength self-healing hydrogels based on strong metal-coordination bonds has emerged as another new research hotspot for balancing the contradiction[14–16]. While the potential toxicity of metal ions reduces the biocompatibility of this type of self-healing hydrogels and severely hinders their applications in biomedicine[17]. At present, the tensile strength of biocompatible self-healing hydrogels that have been reported is usually in the range of 8—280 kPa, among them the hydrogels with high healing efficiency (≥ 80%) usually possess a tensile strength of less than 60 kPa[18–27]. Thus, the key to promoting the application of biocompatible high-strength hydrogels in biomedicine lies in improving their self-healing performance.

Polyvinyl alcohol (PVA) is a water-soluble polyhydroxy polymer with good mechanical strength and biocompatibility[28], which can form hydrogels with good mechanical strength through physical cross-linking. Tannic acid (TA) is a natural water-soluble plant polyphenol compound with good biocompatibility[29]. It has a large number of highly active phenolic hydroxyl groups and can form multiple reversible H bonds with PVA[30–32], which is beneficial for preparing the hydrogel with high tensile strength and self-healing efficiency. However, some reports point out that when the concentration of PVA and TA is high, it is difficult to form a uniform hydrogel network[33]. Because after high concentrations of TA and PVA contact, multitudes of H bonds will be quickly formed, which will lead to the formation of a condensation zone on the surface of the hydrogel, seriously hindering the continuous diffusion of TA in the hydrogel and resulting in a high local TA concentration, which makes the obtained hydrogel precursor uneven and difficult to further gel. In our previous work[34], we have successfully increased the TA content in PVA-TA hydrogel by modifying the preparation condition, and obtained the PVA-TA hydrogel with a tensile strength of 224 kPa and a self-healing efficiency of 87% in 2 h. However, the self-healing hydrogel's tensile strength requires further improvement. Electrostatic interaction is a non-covalent reversible interaction whose bond energy is up to 100–350 kJ/mol[35], much higher than that of the H bond (1.05–62.76 kJ/mol[36]). If the electrostatic interaction can be introduced into the PVA-TA hydrogel, its tensile strength may be effectively improved. Chitosan (CS) is a N-deacetylated derivative of chitin and a natural cationic polysaccharide, obtained from shellfish's shells. It has good biocompatibility, biodegradability and is often used in various tissue engineering materials[37]. CS can form reversible H bonds with PVA and TA. In addition, reversible electrostatic interactions can be formed between CS and TA[38]. Theoretically, self-healing hydrogels with good biocompatibility, high strength, and excellent self-healing efficiency may be obtained by combining PVA, TA, and CS by virtue of the synergistic interactions of physical cross-linking, electrostatic interaction, and reversible hydrogen bonds. Based on the above, a polyvinyl alcohol-chitosan/tannic acid (PVA-CS/TA) hydrogel with good biocompatibility was developed in this paper, and its self-healing efficiency can reach 84% in 2 h. The proposed PVA-CS/TA hydrogel is largely resistant to tension, and the strength can reach 447 kPa, which is significantly higher than that of the reported biocompatible self-healing hydrogels with similar self-healing properties up to now.

Experiments

Materials

The PVA with a degree of polymerization of 1750 ± 50 and a degree of hydrolysis of 99.8–99.9% was purchased from Sinopharm Chemical Reagent Co., Ltd., China. The TA with a molecular weight of 1701 g/mol was purchased from Shanghai Maclean Biochemical Co., Ltd. The CS was purchased from Sinopharm Chemical Reagent Co., Ltd., China. The degree of deacetylation measured by acid–base titration was 81.3%, and the molecular weight measured by gel permeation chromatography (GPC) was 8.75×10^4.

Preparation of PVA-CS/TA hydrogel

The PVA-CS/TA hydrogel was fabricated through the following procedures (as shown in Fig. 1). The chitosan was dissolved in 1.7 wt.% acetic acid solution and stirred continuously for 24 h to obtain a 4.8 wt.% chitosan stock solution. The PVA was dissolved in a mixture of chitosan solution and deionized water, heated and stirred at 100 °C for 2 h to get a PVA and CS mixed solution. Then 50 wt.% TA solution was added and stirred at 100 °C for 1 h. The homogeneous mixture of PVA, CS, and TA was the precursor of PVA-CS/TA hydrogel. The total content of CS and TA was 3 wt.%, the mass ratios were respectively 0:3, 1:2, and 1:1, and the PVA content was 30 wt.%.

The PVA-CS/TA hydrogel precursor was defoamed in a vacuum box for 0.5 h at -0.1 MPa (vacuum pressure gauge). Then the sample was poured into a mold, sealed with plastic wrap to prevent moisture loss, and frozen in a refrigerator at -26 °C for a certain period of time. After that, it was defrosted at room temperature (25 ± 1.5 °C) for 6 h to obtain the hydrogel. The PVA-CS/TA hydrogel specimen was named PVA-CS/TA(m)-(n) to distinguish the mass ratio of CS and TA (m), and the freezing time (n) recorded in minutes. For example, PVA-CS/TA0.5–40 represents 30 wt.% of PVA in the hydrogel, the total content of CS and TA was 3 wt.%, the mass ratio of CS over TA was 0.5, and the freezing time was 40 min. The composition list of PVA-CS/TA hydrogels is shown in Table 1.

The CS/TA mass ratio was kept less than 1 because high CS content will lead to gelation failure since high CS content increases the surface tension of the polymer solution[39]. Moreover, strong H bonds formed quickly between PVA and CS and yielded coacervating layers on the surface of PVA particles, which greatly hampered the continuous diffusion of CS and PVA molecules in the hydrogel precursor[33].

SEM observation

The PVA-CS/TA0-40, PVA-CS/TA0.5–40, and PVA-CS/TA1-40 hydrogels were frozen in liquid nitrogen for 20 min and fractured for the brittle section. It was freeze-dried in a freeze dryer (Beijing Songyuan Huaxing

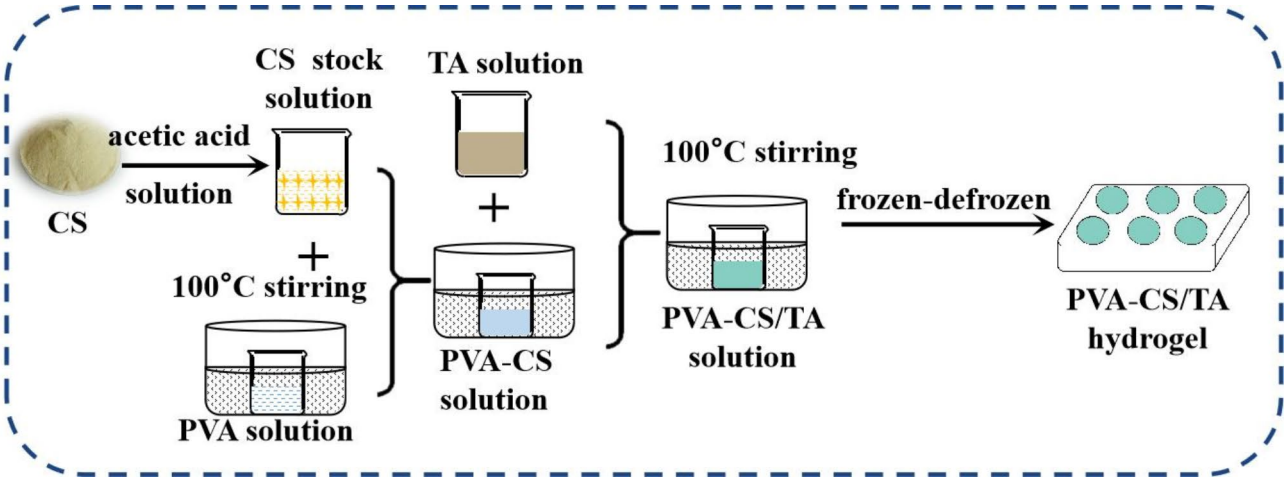

Fig. 1. Schematic presentation of the preparation steps of PVA-CS/TA hydrogel.

Hydrogel	PVA (wt. %)	CS (wt. %)	TA (wt. %)	CS/TA mass ratio	Water (wt. %)	Freezing time (min)
PVA-CS/TA0	30	0	3	0	67	30
						40
						50
PVA-CS/TA0.5		1	2	0.5		30
						40
						50
PVA-CS/TA1		1.5	1.5	1		30
						40
						50

Table 1. The composition of PVA-CS/TA hydrogels.

Technology Co., Ltd., LGJ-10). After spraying gold on the brittle section of the dried sample, it was observed under a scanning electron microscope (FEI Quanta 200, FEI, USA).

Resonance light scattering and thermogravimetric analysis

The aggregation state of the molecules in the solution was analyzed by synchronously scanning the spectrum with a fluorescence spectrophotometer (FP-6500, Jasco) with a 150 W hernia lamp in the range of 200–700 nm ($\lambda_{ex}=\lambda_{em}$, *i.e.*, $\Delta\lambda=0$ nm). The slits for the emitted light and the incident light were both set at 3 nm. The original solution was diluted to have a certain degree of transparency for resonance light scattering (RLS) analysis. The tested solutions were PVA solution (0.3 g/L), TA solution (0.02 g/L), CS solution (0.01 g/L), PVA-CS/TA0 solution (PVA: 0.3 g/L, CS/TA: 0/0.03), PVA-CS/TA0.5 solution (PVA: 0.3 g/L, CS/TA: 0.01 g/L /0.02 g/L), and PVA-CS/TA1 solution (PVA: 0.3 g/L, CS/TA: 0.015 g /L /0.015 g/L).

The thermogravimetric analyzer (TGA 209, NETZSCH) was used to characterize the thermal degradation behaviour of CS, TA, and CS/TA. Appropriate amounts of CS powder, TA powder, and CS/TA powder (obtained by freeze-drying CS/TA solution) were taken, and the thermogravimetric curves of the samples were recorded by TGA from room temperature to 800℃ at a rate of 20℃/min under a nitrogen atmosphere.

Self-healing performance characterization

The self-healing properties of PVA-CS/TA hydrogel were characterized through a combination of qualitative and quantitative methods.

Qualitative characterization

One piece of hydrogel was cut into two halves and horizontally placed together for a simple touch of the cutting surfaces at room temperature without any other intervention. An optical microscope (Shanghai Yongheng Optical Instrument Manufacturing Co., Ltd.) was used to observe the self-healing of the hydrogel at different time intervals.

Quantitative characterization

(I) Dynamic self-healing performance tests: The rheometer (Anton Paar MCR302, Austria) was used to perform the dynamic rheology tests of the PVA-CS/TA hydrogel at 25 °C. A parallel plate (diameter: 25 mm, thickness:

1 mm) was used to monitor the changes in the storage modulus (G') and loss modulus (G''). The amplitude oscillation test was carried out at 1 Hz. The hydrogel on the parallel plate was symmetrically cut into 16 pieces, and the frequency sweeping rheological test was performed immediately after complete self-healing to evaluate the healing properties. The alternate step strain sweeps on the hydrogel were performed by increasing the shear strain from 1% (200 s at each interval) to 100% (100 s at each interval) and then dropping to 1% for 10 times to test the hydrogel's self-healing performance.

(II) Static self-healing performance tests: The hydrogel's self-healing ability was quantitatively evaluated through tensile tests. The tensile experiment was carried out at room temperature on a universal testing machine (C43.104, MTS Systems Co., Ltd.). The tensile strain rate was 400%/min. The sensor range was 500 N. The sampling frequency was 2 Hz. The experimental steps were as follows: First, the original dumbbell-shaped hydrogel (pararllel segment sizes, length: 15 mm, width: 10 mm; thickness: 3 mm) was stretched to break to get the tensile stress–strain data of the original hydrogel. Then the hydrogel sample was cut into two pieces in the middle and then put together for spontaneous healing at room temperature for a certain period of time. The same tensile experiments were performed on healed hydrogel samples to compare their healing performance. For tensile tests, two points were marked on the parallel Sect. (15 mm × 10 mm × 3 mm) of the dumbbell-shaped sample. A high-speed camera (CCD) was used to track the coordinates of the two points during the stretching process to calculate the strain. The self-healing efficiency was equal to the ratio of the tensile strength of the hydrogel after self-healing to the tensile strength of the original hydrogel. In order to study the changes in self-healing efficiency with time, we measured the self-healing rate at 0.5 h, 1 h, 1.5 h, and 2 h.

Infrared spectroscopy observation

The infrared spectra of PVA hydrogel, TA powder, CS powder, PVA-CS hydrogel, PVA-TA hydrogel, dry powder of CS/TA solution, and PVA-CS/TA0.5–40 hydrogel were analyzed through attenuated total reflection Fourier transform infrared spectroscopy (ATR-FTIR, Thermo Fisher Nicolet 6700) in 400 cm^{-1}–4000 cm^{-1}.

Biocompatibility

The cytotoxicity assessment of PVA-CS/TA0.5–40 hydrogel in an vitro setting entailed utilization of the CCK-8 assay and HaCaT cells. The employed HaCaT cells were purchased from the China Center for Type Culture Collection in Wuhan.

The freeze-dried hydrogel was exposed to ultraviolet irradiation for a period of 24 h to sterilize. The preparation of subsequent required extract solution was executed by incorporating the sterilized hydrogel into the culture medium, and the hydrogel weight of culture medium ratio is 20 mg/ml. After that, the resultant solution was subjected to incubation under conditions of 37 °C for a duration of 24 h within an incubator, thereby yielding the extract medium. Then the extract solution was diluted with the culture medium to achieve varying dilutions, namely 10 mg/ml, 1 mg/ml, and 0.1 mg/ml, and designated as C_{10}, C_1, and $C_{0.1}$, respectively. For the cultivation of HaCaT cells, an inoculation was performed into a 96-well plate, with each well receiving an inoculum of 100 µl at a cell density of 5×10^4 cells/ml. Post-inoculation, the plates were maintained under incubation conditions of 37 °C with an atmospheric supplementation of 5% CO_2 for an initial period of 4 h. Following the initial incubation, an additional 100 µl of extract at the aforementioned varying concentrations was introduced to each well, and the culture medium was refreshed every 48 h. Subsequently, at intervals of 1 day, 3 days, and 5 days post-inoculation, 100 µl of fresh medium complemented with 10 µl of the CCK-8 assay reagent (Dojindo, Japan) was introduced into each well. These wells were then subjected to an additional incubation period of 3 h in the dark at a controlled temperature of 37 °C. The quantification of relative cellular viability was achieved by transferring 100 µl of the supernatant to a new, sterile 96-well plate and measuring the optical density at a wavelength of 450 nm using a multi-functional plate reader (Spectrafluor, Australia). The formula for determining relative cell viability was established as follows: Relative cell viability (%) = ($OD_{experiment}$/$OD_{control}$) × 100, where OD represents the optical density, which was derived from the average value garnered from triplicate experiments. Each experimental set was duplicated across three parallel samples for the purpose of statistical reliability.

To facilitate a more direct assessment of the survival state of HaCaT cells, a cohort of cells that had been in cultivation for a period of 5 days was subjected to a series of analytical procedures. Initially, the cells were rinsed with Phosphate-Buffered Saline (PBS) to remove any residual media components. This was followed by an incubation phase at a controlled temperature of 37 °C, which spanned a duration of 15 min, during which the cells were exposed to a live/dead cell detection kit. Subsequently, the cells underwent three iterations of rinsing with PBS to eliminate any unreacted stain, thereby ensuring the clarity of the subsequent microscopic examination. The state of the cells was subsequently scrutinized using a fluorescence microscope (Olympus IX71, Japan). This enabled the differentiation between live and dead cells through distinct colorations, with live cells exhibiting a green fluorescence due to staining with Calcein-AM and dead cells displaying a red fluorescence attributed to Propidium Iodide (PI).

Results and discussion

Micromorphology of the hydrogel

The cross-sectional micromorphology of the hydrogel originated from the SEM images of freeze-dried PVA-CS/TA hydrogel, as shown in Fig. 2. Figure 2a,b are the SEM images of PVA-CS/TA0-40. It can be seen that the cross-section of the PVA-CS/TA0-40 hydrogel presents a highly dense uniform structure with no obvious pores above 1 µm in the microstructure. After the CS is added, the obvious porous structures are presented, as seen in the SEM images of PVA-CS/TA0.5–40 (Fig. 2c,d). It may be that the addition of CS makes the ice crystals produced during the freezing process of hydrogel, which can leave the porous structure in situ in the hydrogel after melting. The PVA macromolecular chain is the formation basis of a three-dimensional network in the

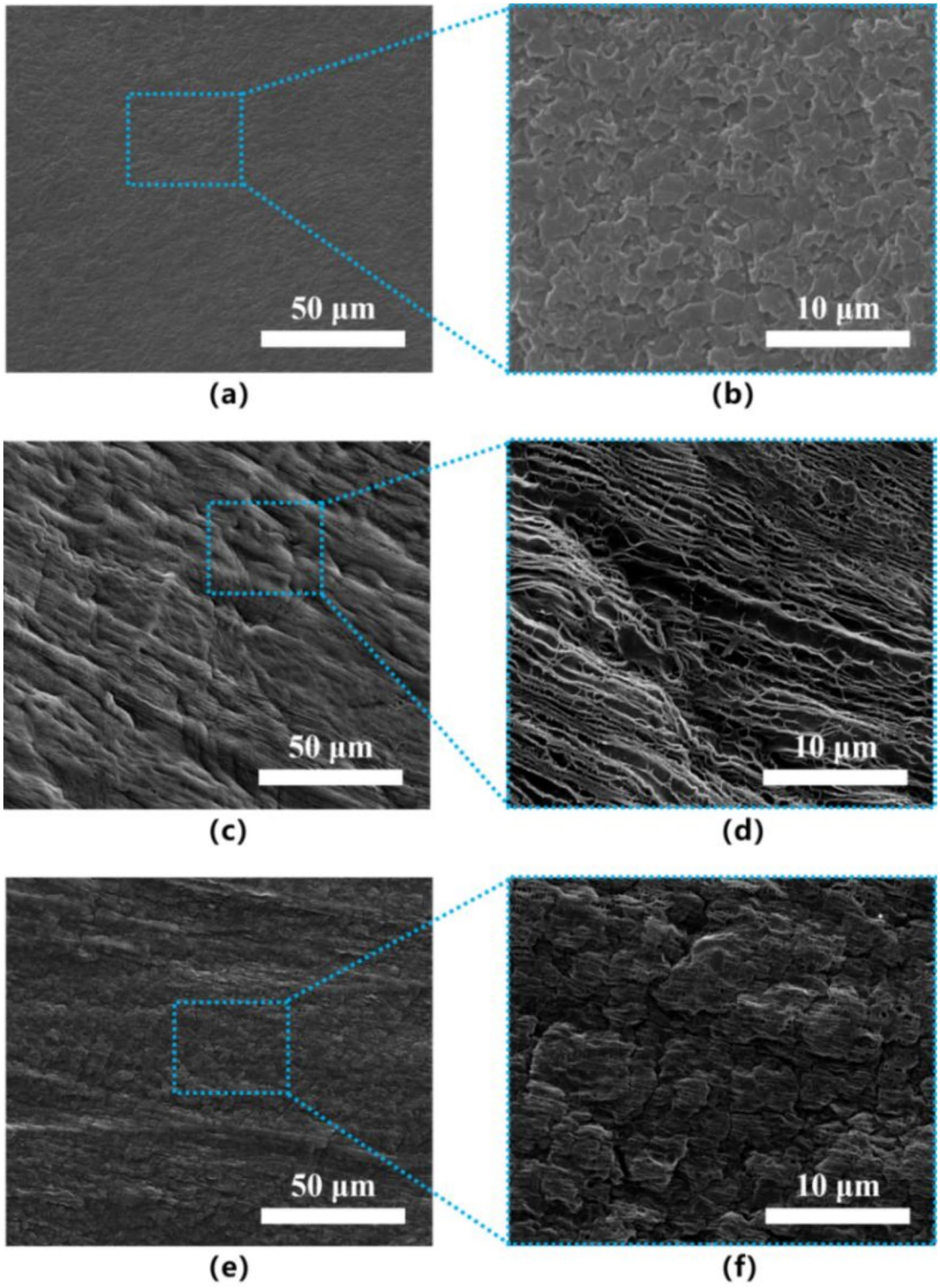

Fig. 2. SEM image of cross-section of PVA-CS/TA hydrogel, magnified 1000 times and 5000 times: (**a**,**b**) for PVA-CS/TA0-40; (**c**,**d**) for PVA-CS/TA0.5–40; (**e**,**f**) for PVA-CS/TA1-40.

hydrogel. The addition of CS will cause further aggregation of PVA molecular chains, forming the rich and poor phase areas of PVA molecular chains in the hydrogel precursor. In the rich phase areas, the formation of ice crystals is hindered. While in the poor phase areas, due to the higher content of water molecules, the ice crystals tend to grow and form porous structures during freeze–thaw crosslinking[40]. In addition, the pore size decreases with the ratio of CS/TA increases, as seen in the SEM images of PVA-CS/TA1-40 (Fig. 2e,f). This may be due to

the further increase of the CS polymer chain number, which leads to the reduction of reversible interactions, against the aggregation of CS and PVA polymer chains.

In order to detect polymer chain aggregation of PVA-CS/TA hydrogel precursors, the resonance light scattering (RLS) is used, as the scattering intensity depends on the degree of polymer chain aggregation[41]. Figure 3 shows the resonance light scattering (RLS) spectra of PVA solution, TA solution, CS solution, and PVA-CS/TA solution. There is almost no light scattering phenomenon in PVA solution, TA solution, and CS solution. When the PVA solution is mixed with TA, the scattering phenomenon of the PVA-CS/TA0 solution is significantly enhanced, and the scattering intensity is much stronger than that of the pure PVA and TA solutions. This indicates that the local aggregation of polymer chains appears in the solution[42]. The formed hydrogen bonds between the PVA and TA in the solution will cause the polymer chains to link closely to form an interlocking structure, increasing the entanglement degree of polymer chains, and resulting in the local aggregation of polymer chains. Since CS can not only form a large number of hydrogen bonds with PVA and TA but also electrostatic interactions with TA[38], further increasing the local aggregation of polymer chains, the partial replacement of TA by CS will incur a further increase of the scattering intensity of PVA-CS/TA0.5 and PVA-CS/TA1 solutions, as shown in Fig. 3.

Self-healing properties

To elucidate the influence of varying constituents on the self-healing capabilities of PVA-CS/TA hydrogels, an investigation was conducted, measuring the self-healing efficacy through tensile testing. Figure 4a,c,e delineate the tensile stress–strain curves for the pristine PVA-CS/TA hydrogels with distinct cross-linking times and composition ratios (represented by solid lines), juxtaposed with their counterparts post self-healing at ambient temperature for a period of two hours following fracture (indicated by dotted lines). Figure 4b,d,f offer a comparative analysis of the original and post-self-healing tensile strengths of the hydrogels under scrutiny.

The observations presented in Fig. 4a,b reveal a progressive increment in tensile strength of the PVA-CS/TA0 hydrogel from 222 to 778 kPa, concomitant with a decline in self-healing efficiency from 86 to 21%. This phenomenon can be attributed to the semi-crystalline nature of PVA, where freeze–thaw crosslinking

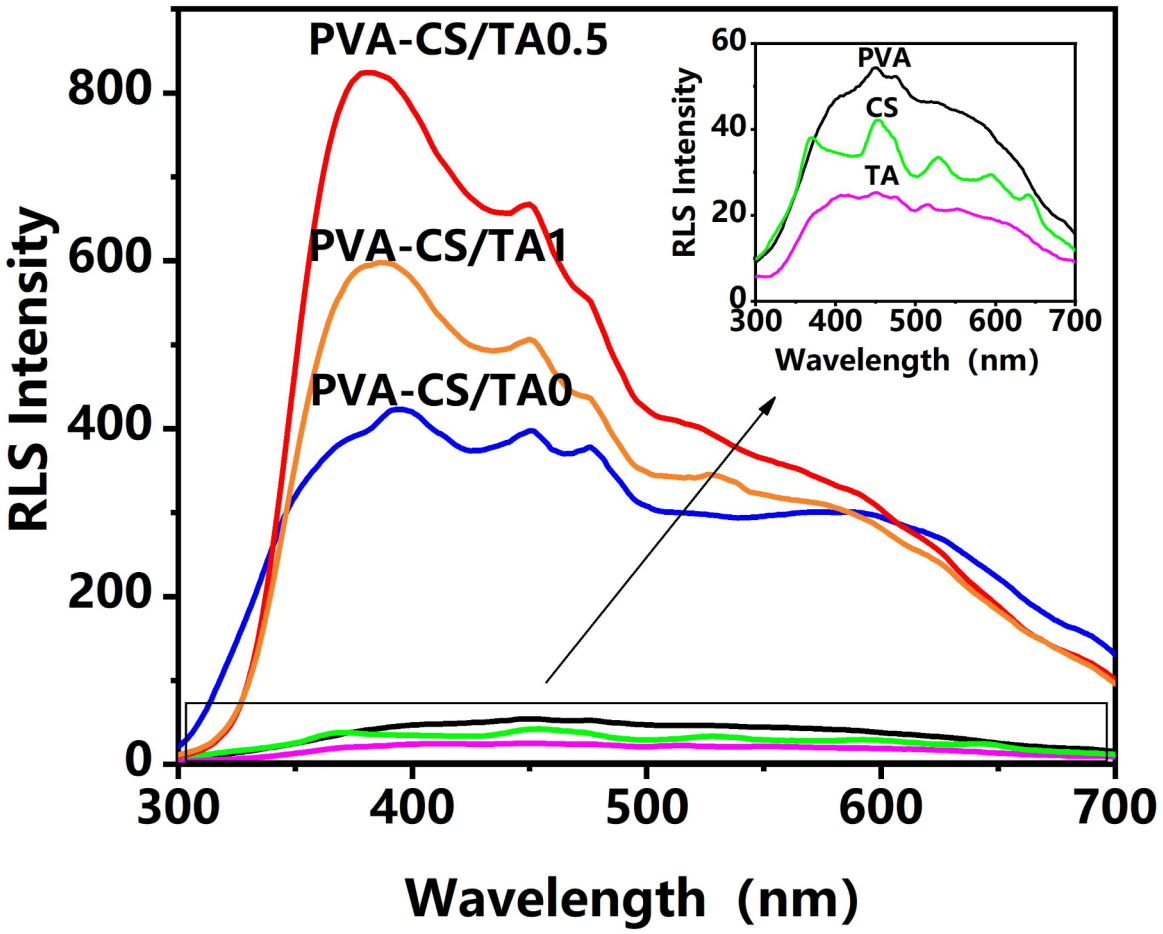

Fig. 3. Resonance light scattering (RLS) spectra of PVA solution, TA solution and PVA-TA solutions with different TA content.

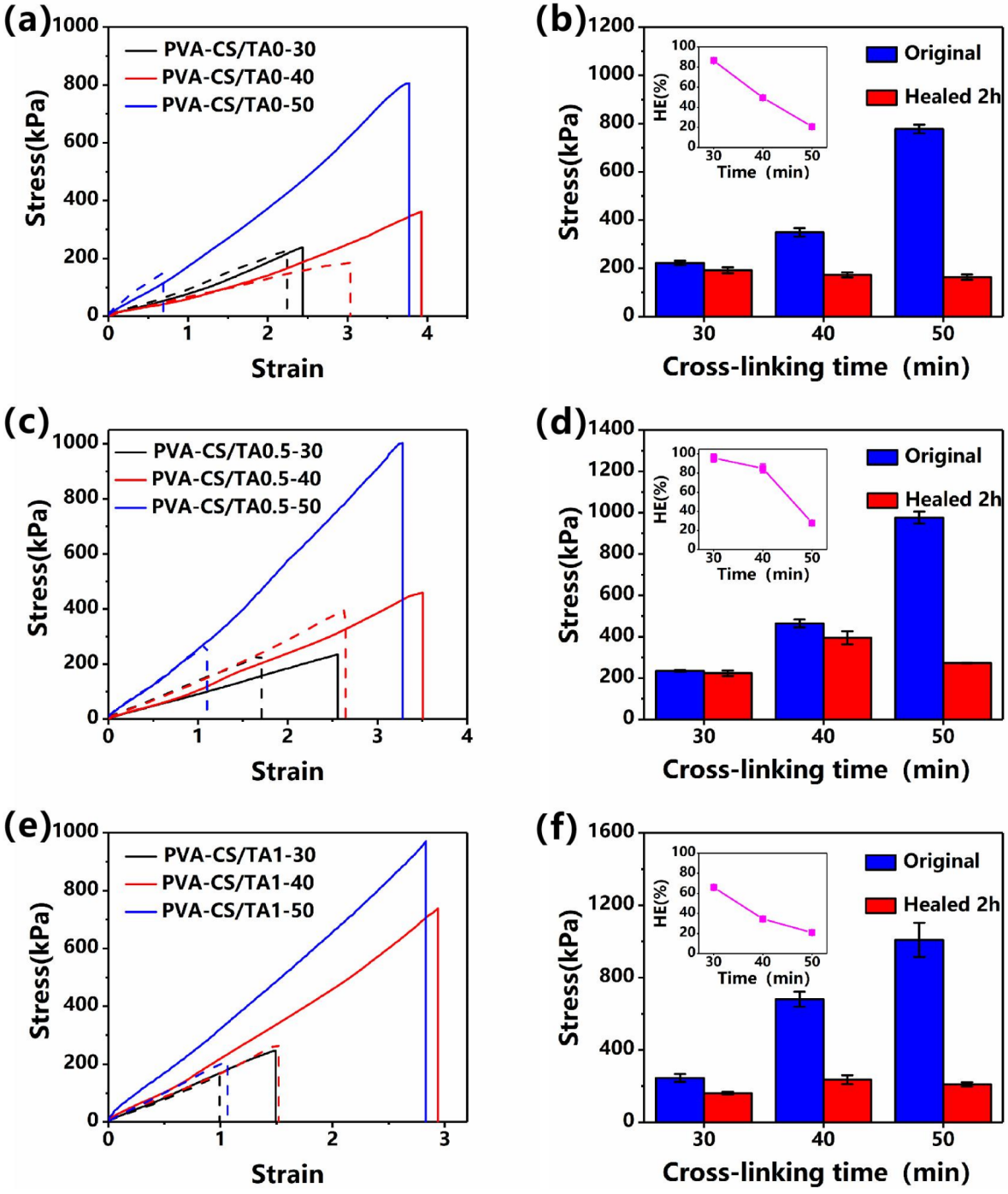

Fig. 4. The tensile stress–strain curves and the relationship between the tensile strength and cross-linking times of the original hydrogels and the self-healed hydrogels with a self-healing time of 2 h: (**a**,**b**) for PVA-CS/TA0; (**c**,**d**) for PVA-CS/TA0.5; (**e**,**f**) for PVA-CS/TA1. In the graphical representations of tensile stress–strain curves, the solid lines represent the original hydrogels and the dashed lines represent the self-healed hydrogels. The insets show the healing efficiency of hydrogels with different cross-linking time, N = 3.

procedures induce the formation of microcrystals within the hydrogel, which act as cross-linking junctions. And these junctions facilitate a three-dimensional rigid network through the interconnection of PVA polymer chains by these crystalline cross-links[43]. The crystals or crystal size within the PVA-CS/TA0 hydrogel expands with extended freezing periods, bolstering the mechanical strength of the hydrogel. Although this results in a more robust network structure, it does not change the number of reversible interaction of polymer chains within the PVA-CS/TA0 hydrogel, but reduces the polymer chains' mobility. Since the self-healing performance is influenced by the number of reversible interactions and the fluidity of polymer chains, the decrease in polymer

chains' mobility without a change of the number of reversible interaction results in the decrease in self-healing performance. When a portion of CS is supplanted by TA, as illustrated in Fig. 4, the tensile strengths of PVA-CS/TA0.5 (234 kPa to 976 kPa) and PVA-CS/TA1 hydrogels (245 kPa to 1008 kPa) are comparable but surpass that of PVA-CS/TA0. This may be due to the introduction of TA, which forms H bonds with stronger bond energy between PVA, TA, and CS[44]. Generally, shorter bond length and larger bond angle result in higher H-bond energy[45]. Through molecular simulation, Guo et al.[44] showed that the H bonds between PVA, TA and CS have shorter bond length and larger bond angle than those between the different molecular chains of PVA, and PVA and CS. Thus, the introduction of TA increases the tensile strength of PVA-CS/TA hydrogels. The self-healing performance of the PVA-CS/TA0.5 hydrogel (28% and 96%) exceeds that of both PVA-CS/TA0 (21% to 86%) and PVA-CS/TA1 (21% to 66%). Since CS can not only form H bonds with PVA and TA but also form electrostatic interactions with TA[38], and the bond energy of electrostatic interactions (100–350 kJ/mol[35]) is much higher than that of H bonds (1.05–62.76 kJ/mol[36]), which is beneficial for improving the mechanical strength and self-healing performance of the PVA-CS/TA hydrogels. On the other hand, the increase in mechanical strength will reduce the mobility of polymer chains within the hydrogel, resulting in a decrease in hydrogel's self-healing performance. Therefore, there will be a balance point where PVA-CS/TA hydrogel has both high mechanical strength and good self-healing performance. As seen in Fig. 4d, the PVA-CS/TA0.5 hydrogel with a cross-linking time of 40 min possesses the best mechanical strength and self-healing performance among the synthesized PVA-CS/TA hydrogels.

To investigate the microscopic self-healing behavior of the PVA-CS/TA0.5 hydrogel with a cross-linking time of 40 min (denoted as PVA-CS/TA0.5–40), microscopic examination was conducted to assess the state of gel cohesion over varying intervals post-incision. The microscopic images are depicted in Fig. 5a–c. Initially, when the incised PVA-CS/TA0.5–40 hydrogels are juxtaposed, a discernible fissure, approximately 630 μm in breadth, is observed at the interface of the separated segments, as illustrated in Fig. 5a. But the progressive constriction of the initial crack is evident after intervals of 1 h and 2 h, as shown in Fig. 5b,c, indicating the hydrogel has good self-healing performance.

To investigate the self-healing characteristics of PVA-CS/TA0.5–40 hydrogel, the rheological measurements were conducted. The results, as depicted in Fig. 5d, show that the storage modulus (G') and loss modulus (G") of the PVA-CS/TA0.5–40 hydrogel remain stable within the critical strain range of 25.1%. In addition, within the shear strain range of 0.01% to 25.1%, the G' surpasses the G", indicating that the hydrogel's behavior in this range predominantly exhibit linear viscoelastic. When the applied strain is further increases to over the critical strain value, the G' and G" decrease rapidly, suggesting that the three-dimensional network of the hydrogel begins to collapse. Figure 5e displays the G' and G" of PVA-CS/TA0.5–40 hydrogel under the time scanning. It can be seen that upon subjecting the hydrogel to eight cycles of alternating shear strains of 1% and 100%, the hydrogel can swiftly return to its pre-strain state, suggesting an ability to rapidly regenerate its network structure following multiple high strain damages. Figure 5f exhibits the detail of fourth cycle of the G' and G" under the time scanning, showing a pronounced alteration in both G' and G" as the shear strain escalates from 1 to 100%. To be specific, the G' diminishes from 7.8 kPa to 5.2 kPa, while the G" ascends from 1.3 kPa to 1.9 kPa, indicating temporary disruption to the hydrogel's network. Nonetheless, upon release from the 100% shear strain, the deviation in G' and G" from their initial values is swiftly minimized, with a reduction to 0.8% and 5.6% within 35 s, suggesting that the reversible H bonds and electrostatic attractions within the hydrogel are spontaneously reestablished immediately at ambient temperature. The results of frequency scanning displayed in Fig. 5g show that the values of G' of the original hydrogel and self-healing hydrogel are all larger than the G" values, and the G' and G" values post self-healing hydrogel are closely approximate those of the original hydrogel, implying that both the original hydrogel and self-healing hydrogel show elastic behavior, and the internal structure of the self-healing hydrogel are restored well.

To quantitatively characterize the static self-healing efficiency of PVA-CS/TA0.5–40 hydrogel, a tensile test is conducted, and the results are exhibited in Fig. 5h. The restoration of tensile strength of the hydrogel was observed to progress with the duration of the self-healing period, with the resulting stress–strain profiles of the self-healed specimens closely approximating that of the original hydrogel. Concurrently, the rate of self-repairing declines as the healing interval extends, yet the self-healing efficiency is still commendable, reaching up to 84% within a 2-h time frame, as illustrated in Fig. 5i. It is worth mentioning that due to the contradiction between mechanical strength and self-healing efficiency, the strength of the reported biocompatible self-healing hydrogels with a self-healing efficiency greater than 70% is less than 300 kPa, and the self-healing time is usually as long as 24–48 h[18–27]. However, the strength and self-healing efficiency of the PVA-CS/TA0.5–40 hydrogel prepared here are 447 kPa and 84% with a self-healing time of 2 h, which is significantly better than that of the reported self-healing hydrogels up to now (as summarized in Table 2).

Self-healing mechanism

The molecular structures of PVA, TA, and CS are shown in Fig. 6a. It can be seen that tannic acid (TA) is a natural polyphenol polymer with 25 hydroxyl groups and 10 carbonyl groups for each molecule, which can form strong H bonds with PVA through the highly active phenolic hydroxyl group. Chitosan (CS) is a natural carbohydrate polymer with a large number of free amino groups in its molecular structure. When the pka value of the solution is lower than 6.2, the amino group ($-NH_2$) on the CS molecular chain can unite with the hydrogen ion in the solution, protonating as $-NH^{3+}$[48]. CS can form reversible H bonds and electrostatic interaction with TA, and form H bonds with PVA. In addition, H bonds can be formed between the hydroxyl groups of PVA.

Figure 6b depicts a schematic diagram of the PVA-CS/TA hydrogel network. The H bonds (brown dashed line) polymerize among PVAs (green wavy line) in situ. TA (pink circle) and CS (blue wavy line) connect on PVA polymer chain with H bonds. The TA and CS are connected through the H bond and electrostatic attraction (pink dotted line). Overall, there are two reversible non-covalent bonds in the PVA-CS/TA hydrogel: one is the H

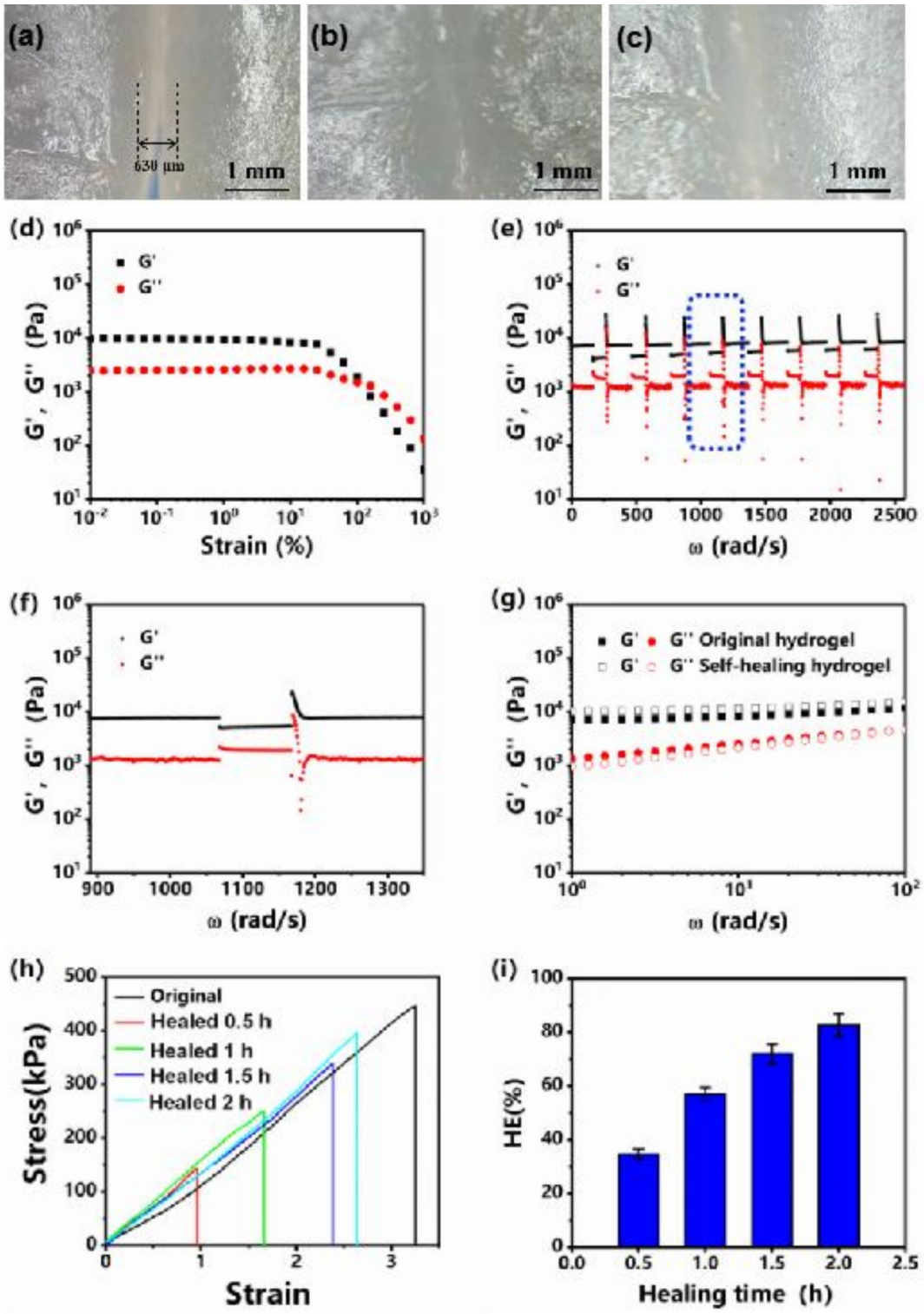

Fig. 5. The self-healing performance of PVA-CS/TA0.5–40. Microscopic images under different self-healing time (**a**) 0 h, (**b**) 1 h, (**c**) 2 h; (**d**) the storage modulus G' and loss modulus G'' under the strain scanning; (**e**) G' and G'' under the time scanning; (**f**) detail of the fourth cycle in figure (**e**); (**g**) G' and G'' of the original hydrogel and the self-healed hydrogel (f = 1.0 Hz; strain: 1.0%); (**h**) the tensile stress–strain curves under different self-healing time of 0.5 h, 1 h, 1.5 h, and 2 h, (**i**) the relationship between the self-healing efficiency and the self-healing time during the healing process, N = 3.

Type of hydrogel	Tensile strength	Self-healed time	Self-healing efficiency	Ref
PVA-CS/TA	447 kPa	2 h	84%	This paper
PVA	278 kPa	48 h	72%	[8]
PVA-TA	224 kPa	2 h	87%	[34]
Zr-NC gel	195 kPa	12 h	75%	[46]
PVA/PAM-PAA	160 kPa	12 h	37%	[26]
CNF-PPy/PB	63 kPa	20 s	97%	[47]
PNIPAM-PAM-clay	60 kPa	150 h	90%	[18]
β-CD-AOI$_2$-A-TEG-Ad	28 kPa	1 h	63%	[25]
Agarose/PVA	25 kPa	10 s	100%	[21]
DF-PEG	23 kPa	24 h	100%	[20]
PDA-PGO-PAM	21 kPa	24 h	62%	[22]
PDA-talc-PAM	8.5 kPa	2 h	60%	[3]
PDA-PAM	8 kPa	2 h	98%	[19]

Table 2. Summary of properties of biocompatible autonomic self-healing hydrogels.

bond between PVA, CS, and TA, and the other is the electrostatic interaction between CS and TA. The association and dissociation speed of hydrogen bonds is relatively fast, usually on the time scale of sub-picosecond to picosecond[49]. The bonding strength of electrostatic attraction (100–350 kJ/mol) is usually higher than that of the H bond (1.05–62.76 kJ/mol)[35,36]. The synergistic effect of the H bonds and electrostatic interactions yields high-strength hydrogels with more efficient self-healing properties. Even in the PVA-CS/TA hydrogel with high mechanical strength and low molecular chain mobility, it still has good self-healing properties and can quickly self-heal without any external stimulation.

In order to identify the intermolecular interactions in polymer blends, the FTIR analysis is used, and the FTIR spectra in the wavenumber range of 400 cm^{-1}—4000 cm^{-1} of PVA, TA, CS, PVA-TA, CS/TA, PVA-CS, and PVA-CS/TA hydrogels are given in Fig. 7. It can be seen that the characteristic peaks of -OH stretching in the pure PVA, TA, and CS are shown at 3293 cm^{-1}, 3335 cm^{-1}, and 3298 cm^{-1}, respectively. After TA is added to PVA, the characteristic peaks of -OH stretching in the PVA-TA, CS/TA, PVA-CS, and PVA-CS/TA0.5–40 are shifted to lower wave numbers of 3275 cm^{-1}, 3287 cm^{-1}, 3285 cm^{-1}, and 3283 cm^{-1}, respectively, indicating that H bonds are formed between PVA, TA, and CS. This is because that the formation of intramolecular or intermolecular hydrogen bonds will reduce the force constant of the chemical bonds, shifting their vibration frequencies to a lower wavenumber[31]. In addition, a broad peak is shown at 3298 cm^{-1} in the CS spectrum, which is attributed to the overlap of the -NH stretching of the primary amino group and the -OH stretching vibration. 2875 cm^{-1} is the characteristic peak of -CH, and 1650 cm^{-1} is the characteristic peak of secondary amide band (amide I) carbonyl stretching. 1598 cm^{-1} is the characteristic infrared peak of -NH_2, which is characteristic of chitosan[50]. 1421 cm^{-1} and 1382 cm^{-1} are -CH_3 symmetrical deformation modes. Comparing with the spectrum of PVA-CS hydrogel, after CS protonation, the characteristic peak of 1650 cm^{-1} shifts to 1640 cm^{-1}, and the characteristic peak of 1598 cm^{-1} shifts to 1567 cm^{-1}, which proves the protonation of chitosan NH_3^+[51]. Since the CS amino group is positively charged after protonation and the TA, a common anionic polyelectrolyte, is negatively charged after being dissociated. Driven by the reversible electrostatic interaction between the opposite charges of TA and CS, amphoteric materials can be easily attracted by electrostatic interaction, fusing the boundaries of the hydrogel to realize the self-healing properties of the hydrogel.

The thermal stability of CS, TA, and CS/TA was characterized by thermogravimetric analysis, and the thermogravimetric curves are shown in Fig. 8. It can be seen that both CS, TA, and CS/TA have a certain mass loss in the range of 50–100℃, which may be ascribed to the evaporation of water in the samples[52]. After that, a mass equilibrium stage occurs at 100–200℃, and the temperature of the equilibrium stage of CS/TA is significantly higher than that of CS and TA, suggesting that the CS/TA has a stronger thermal stability, which may be due to the strong physical interaction (electrostatic interactions and H bonds) formed between CS and TA.

Biocompatibility

In order to check the biocompatibility of the PVA-CS/TA0.5–40 hydrogel, the cytotoxicity was tested on human immortalized epidermal cells (HaCat). The CCK-8 results in Fig. 9a show the toxicity levels of PVA-CS/TA hydrogel extracts at different concentrations. When the concentration of the extract is 10 mg/mL, 1 mg/mL or 0.1 mg/mL, the HaCat cell viability of the PVA-CS/TA hydrogel is higher than 95% after 1 d, 3 d, and 5 d, indicating the growth of HaCat cells is good. In order to observe and analyze the differences more clearly, the live-dead fluorescence microscope analysis was carried out. After culturing the cells with different concentrations of PVA-CS/TA hydrogel extracts for 5 d. After staining with Calcein-AM and PI, live cells are stained green, and dead cells are stained red. It can be seen from the fluorescent staining results that only a few cells died after culturing with PVA-CS/TA hydrogel extract for 5 d (as shown in Fig. 9b). This result is consistent with the results of CCK-8, indicating that PVA-CS/TA hydrogels (less than 10 mg/mL) have negligible cytotoxicity to HaCat cells.

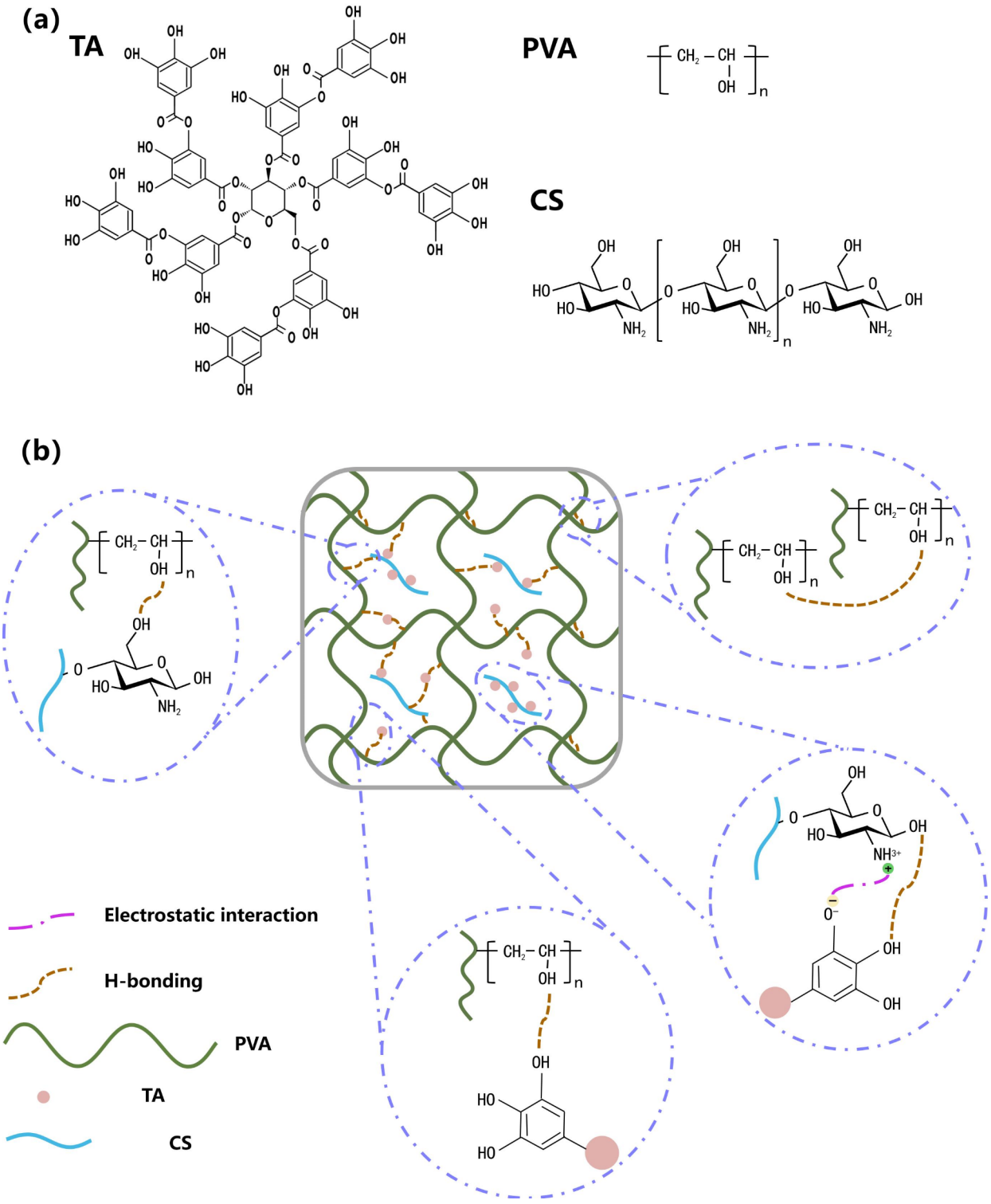

Fig. 6. (**a**) The molecular structure of PVA, TA and CS, (**b**) the schematic diagram of the structure of PVA-CS/TA hydrogel.

Conclusion

The CS with good biocompatibility was introduced into PVA-TA hydrogel, and the effects of the mass ratios of CS and TA (CS/TA) and cross-linking time on the tensile strength and self-healing efficiency of PVA-CS/TA hydrogels were investigated, and the self-healing mechanisms were also discussed. The results suggest that with an increase of cross-linking time, the tensile strength of PVA-CS/TA hydrogel increases, while the self-healing efficiency decreases. It is because the PVA hydrogels prepared by the freeze–thaw crosslinking method will

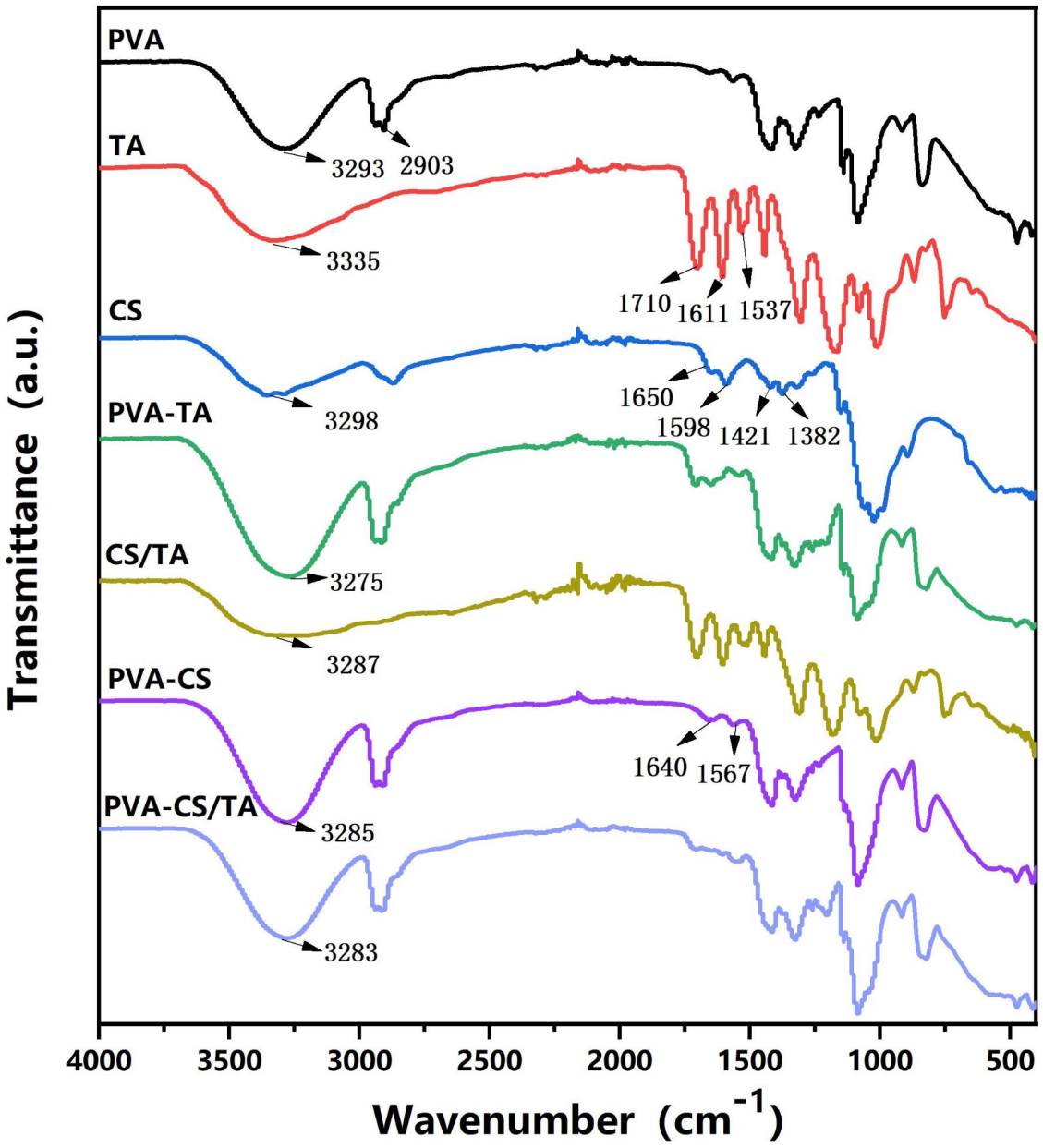

Fig. 7. FTIR spectra of PVA, TA, PVA-CS/TA0.5–40.

produce microcrystals, which acts as crosslinking points to link PVA polymer chains into three-dimensional rigid networks. And the microcrystals will increase with the increase of crosslinking time, resulting in the enhancement of the tensile strength. The stronger tensile strength makes the hydrogel network more stable and limits the polymer chain mobility, which leads to the decrease of self-healing efficiency of the hydrogel. In addition, with the increase of the mass ratios of CS/TA, the tensile strength of PVA-CS/TA hydrogel increases, while the self-healing efficiency increases first and then decreases. Since CS can not only form reversible H bonds with PVA and TA but also form reversible electrostatic interactions with TA. The bond energy of the electrostatic interaction formed between CS and TA is much stronger than that of the H bond, improving the tensile strength and self-healing efficiency of the hydrogels. On the other hand, the increases of tensile strength can inhibit polymer chains mobility, resulting in the decrease of the self-healing efficiency. Thus, the self-healing efficiency increases first and then decreases with the increases of the mass ratios of CS/TA. It is worth pointing out that the tensile strength and self-healing efficiency of the prepared PVA-CS/TA0.5–40 hydrogel are 447 kPa and 84% in 2 h, which is much better than that of the reported autonomous self-healing hydrogels with high biocompatibility.

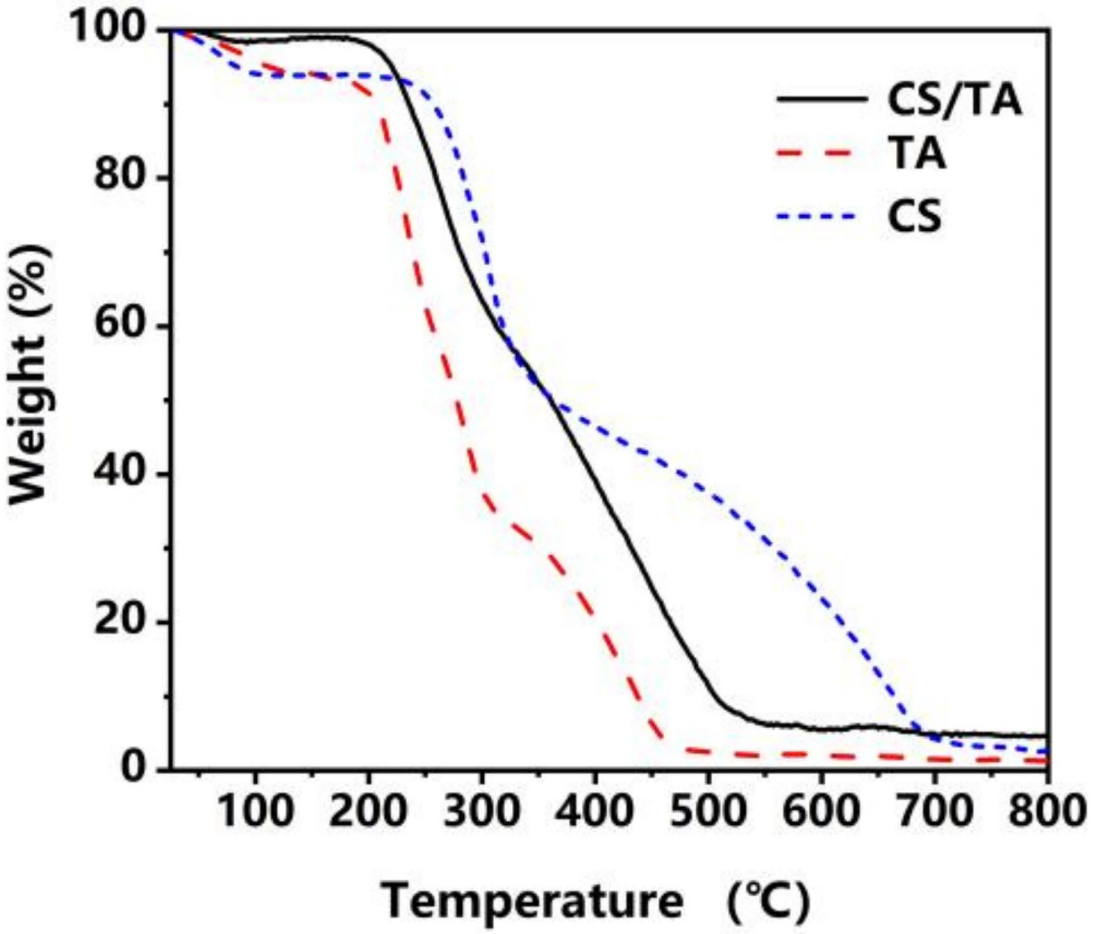

Fig. 8. CS/TA, TA and CS thermogravimetric analysis curves.

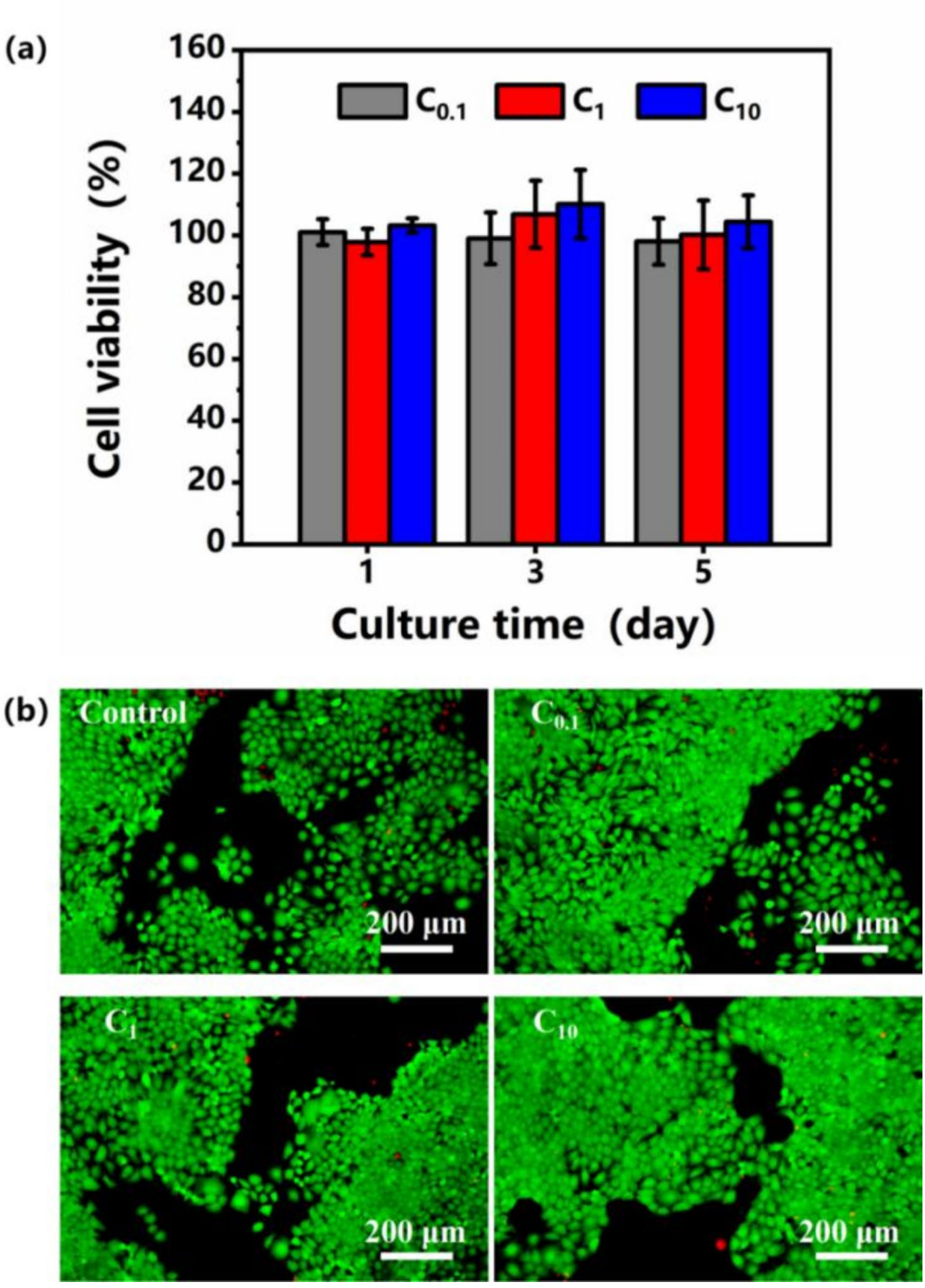

Fig. 9. (**a**) Viabilities of HaCaT cells measured by the CCK-8 assay at 1 d, 3 d and 5 d after co-culture with different concentrations of PVA-CS/TA0.5–40 hydrogel extracts. The data express as the mean ± standard deviation (SD) derived from triplicate experiments. (**b**) Fluorescence images of HaCaT cells stained with Calcein-AM (green) and PI (red) after incubation with different concentrations of PVA-CS/TA0.5–40 hydrogel extracts for 5 d.

Data availability

The datasets used and/or analysed during the current study are availability from the corresponding author on reasonable request.

Received: 22 July 2024; Accepted: 1 January 2025
Published online: 13 January 2025

References

1. Haque, Md. A., Kurokawa, T. & Gong, J. P. Super tough double network hydrogels and their application as biomaterials. *Polymer* **53**, 1805–1822 (2012).
2. Caló, E. & Khutoryanskiy, V. V. Biomedical applications of hydrogels: A review of patents and commercial products. *Eur. Polym. J.* **65**, 252–267 (2015).
3. Jing, X. et al. Highly stretchable and biocompatible strain sensors based on mussel-inspired super-adhesive self-healing hydrogels for human motion monitoring. *ACS Appl. Mater. Interfaces* **10**, 20897–20909 (2018).
4. Wang, Y., Li, Z. & Hu, Q. Emerging self-regulated micro/nano drug delivery devices: A step forward towards intelligent diagnosis and therapy. *Nano Today* **38**, 101127–101127 (2021).
5. Li, X. & Su, X. Multifunctional smart hydrogels: Potential in tissue engineering and cancer therapy. *J. Mater. Chem. B* **6**, 4714–4730 (2018).
6. Li, X., Yang, Q., Zhao, Y., Long, S. & Zheng, J. Dual physically crosslinked double network hydrogels with high toughness and self-healing properties. *Soft Matter* **13**, 911–920 (2017).
7. Liu, J., Song, G., He, C. & Wang, H. Self-healing in tough graphene oxide composite hydrogels. *Macromol. Rapid Commun.* **34**, 1002–1007 (2013).
8. Zhang, H., Xia, H. & Zhao, Y. Poly(vinyl alcohol) hydrogel can autonomously self-heal. *ACS Macro Lett.* **1**, 1233–1236 (2012).
9. Yang, L., Lu, X., Wang, Z. & Xia, H. Diels-Alder dynamic crosslinked polyurethane/polydopamine composites with NIR triggered self-healing function. *Polym. Chem.* **9**, 2166–2172 (2018).
10. Yang, L., Wang, Z., Fei, G. & Xia, H. Polydopamine particles reinforced poly(vinyl alcohol) hydrogel with NIR light triggered shape memory and self-healing capability. *Macromol. Rapid Comm.* **38** (2017).
11. Rong, Q. et al. Anti-freezing, conductive self-healing organohydrogels with stable strain-sensitivity at subzero temperatures. *Angew. Chem. Int. Ed.* **56**, 14159–14163 (2017).
12. Yuan, N. et al. Dual physically cross-linked double network hydrogels with high mechanical strength, fatigue resistance, notch-insensitivity, and self-healing properties. *ACS Appl. Mater. Interfaces* **8**, 34034–34044 (2016).
13. Hohlbein, N., Shaaban, A. & Schmidt, A. Remote-controlled activation of self-healing behavior in magneto-responsive ionomeric composites. *Polymer* **69**, 301–309 (2015).
14. Wang, S., Yuanfei Lv, Feng, S., Li, Q. & Zhang, T. Bimetallic ions synergistic cross-linking high-strength rapid self-healing antibacterial hydrogel. *Polym. Eng. Sci.* **59**, 919–927 (2018).
15. Darabi, M. A. et al. Skin-inspired multifunctional autonomic-intrinsic conductive self-healing hydrogels with pressure sensitivity, stretchability, and 3D printability. *Adv. Mater.* **29**, 1700533 (2017).
16. Kang, M. et al. Template method for dual network self-healing hydrogel with conductive property. *Mater. Des.* **148**, 96–103 (2018).
17. Saleem, M. et al. Facile synthesis, cytotoxicity and bioimaging of Fe^{3+} selective fluorescent chemosensor. *Bioorgan. Med. Chem.* **22**, 2045–2051 (2014).
18. Wang, T. et al. Notch insensitive and self-healing PNIPAm–PAM–clay nanocomposite hydrogels. *Soft Matter* **10**, 3506–3512 (2014).
19. Han, L. et al. Tough, self-healable and tissue-adhesive hydrogel with tunable multifunctionality. *NPG Asia Mater.* **9**, e372 (2017).
20. Zhang, X. et al. Enzyme-regulated fast self-healing of a pillararene-based hydrogel. *Biomacromolecules* **18**, 1885–1892 (2017).
21. Chen, W.-P., Hao, D., Hao, W. J., Guo, X. & Jiang, L. Hydrogel with ultrafast self-healing property both in air and underwater. *ACS Appl. Mater. Interfaces* **10**, 1258–1265 (2018).
22. Han, L. et al. A mussel-inspired conductive, self-adhesive, and self-healable tough hydrogel as cell stimulators and implantable bioelectronics. *Small* **13**, 1601916 (2016).
23. Gulyuz, U. & Okay, O. Self-healing polyacrylic acid hydrogels. *Soft Matter* **9**, 10287–20193 (2013).
24. Shao, C., Wang, M., Chang, H., Xu, F. & Yang, J. A Self-healing cellulose nanocrystal-poly(ethylene glycol) nanocomposite hydrogel via Diels-Alder click reaction. *ACS Sustain. Chem. Eng.* **5**, 6167–6174 (2017).
25. Wang, Z. et al. A rapidly self-healing host-guest supramolecular hydrogel with high mechanical strength and excellent biocompatibility. *Angew. Chem. Int. Ed.* **57**, 9008–9012 (2018).
26. Gong, Z. et al. High-Strength, tough, fatigue resistant, and self-healing hydrogel based on dual physically cross-linked network. *ACS Appl. Mater. Interfaces* **8**, 24030–24037 (2016).
27. Gulyuz, U. & Okay, O. Self-Healing poly(acrylic acid) hydrogels with shape memory behavior of high mechanical strength. *Macromolecules* **47**, 6889–6899 (2014).
28. Kurt, S. B. & Sahiner, N. Chitosan based fibers embedding carbon dots with anti-bacterial and fluorescent properties. *Polym. Compos.* **42**, 872–880 (2020).
29. Ari, B., Sahiner, M., Demirci, S. & Sahiner, N. Poly(vinyl alcohol)-tannic acid cryogel matrix as antioxidant and antibacterial material. *Polymers* **14**, 70 (2021).
30. Fan, H., Wang, J. & Jin, Z. Tough, swelling-resistant, self-healing, and adhesive dual-cross-linked hydrogels based on polymer–tannic acid multiple hydrogen bonds. *Macromolecules* **51**, 1696–1705 (2018).
31. Chen, Y.-N. et al. Poly(vinyl alcohol)–tannic acid hydrogels with excellent mechanical properties and shape memory behaviors. *ACS Appl. Mater. Interfaces* **8**, 27199–27206 (2016).
32. Xu, R. et al. High strength astringent hydrogels using protein as the building block for physically cross-linked multi-network. *ACS Appl. Mater. Interfaces* **10**, 7593–7601 (2017).
33. Chen, Y.-N., Jiao, C., Zhao, Y., Zhang, J. & Wang, H. Self-Assembled polyvinyl alcohol–tannic acid hydrogels with diverse microstructures and good mechanical properties. *ACS Omega* **3**, 11788–11795 (2018).
34. Huang, J. et al. Biocompatible autonomic self-healing PVA-TA hydrogel with high mechanical strength. *Macromol. Chem. Phys.* **222**, 2100061 (2021).
35. Casas-Hinestroza, J. L., Bueno, M., Ibáñez, E. & Cifuentes, A. Recent advances in mass spectrometry studies of non-covalent complexes of macrocycles—A review. *Anal. Chim. Acta* **1081**, 32–50 (2019).
36. Ryan, L. & Norris, R. Cambridge International AS and a Level Chemistry Coursebook with CD-ROM. (Cambridge University Press, 2014).
37. Çay, A., Miraftab, M. & Kumbasar, E. P. Characterization and swelling performance of physically stabilized electrospun poly(vinyl alcohol)/chitosan nanofibres. *Eur. Polym. J.* **61**, 253–262 (2014).
38. An, X., Kang, Y. & Li, G. The interaction between chitosan and tannic acid calculated based on the density functional theory. *Chem. Phys.* **520**, 100–107 (2019).
39. Torres-Giner, S., Ocio, M. J. & Lagaron, J. M. Development of active antimicrobial fiber-based chitosan polysaccharide nanostructures using electrospinning. *Eng. Life Sci.* **8**, 303–314 (2008).
40. Li, X., Wu, W. & Liu, W. Synthesis and properties of thermo-responsive guar gum/poly(N-isopropylacrylamide) interpenetrating polymer network hydrogels. *Carbohydr. Polym.* **71**, 394–402 (2008).
41. Yang, K. et al. Competition between motion constraint and aggregation of macromolecular chains in poly(vinyl methyl ether)/poly(ethylene oxide) aqueous solution during phase transition. *Macromol. Chem. Phys.* **213**, 1735–1741 (2012).

42. Li, Y. et al. Macromolecular aggregation of aqueous polyacrylic acid in the presence of surfactants revealed by resonance Rayleigh scattering. *Macromolecules* **41**, 4873–4880 (2008).
43. Hong, K. H. Preparation and properties of polyvinyl alcohol/tannic acid composite film for topical treatment application. *Fiber Polym.* **17**, 1963–1968 (2016).
44. Guo, W. et al. Chitosan/polyvinyl alcohol/tannic acid multiple network composite hydrogel: preparation and characterization. *Iran. Polym. J.* **30**, 1159–1168 (2021).
45. Zhang, Y. et al. Structural and hydrogen bond analysis for supercritical ethanol: A molecular simulation study. *J. Supercrit. Fluid.* **36**, 145–153 (2005).
46. Jiang, H. et al. Room-temperature self-healing tough nanocomposite hydrogel crosslinked by zirconium hydroxide nanoparticles. *Compos. Sci. Technol.* **140**, 54–62 (2017).
47. Ding, Q. et al. Nanocellulose-mediated electroconductive self-healing hydrogels with high strength, plasticity, viscoelasticity, stretchability, and biocompatibility toward multifunctional applications. *ACS Appl. Mater. Interfaces* **10**, 27987–28002 (2018).
48. Tang, Y.-F., Du, Y.-M., Hu, X.-W., Shi, X.-W. & Kennedy, J. F. Rheological characterisation of a novel thermosensitive chitosan/poly(vinyl alcohol) blend hydrogel. *Carbohydr. Polym.* **67**, 491–499 (2007).
49. Rabideau, B. D. & Ismail, A. E. Mechanisms of hydrogen bond formation between ionic liquids and cellulose and the influence of water content. *Phys. Chem. Chem. Phys.* **17**, 5767–5775 (2015).
50. Costa-Júnior, E. S., Barbosa-Stancioli, E. F., Mansur, A. A. P., Vasconcelos, W. L. & Mansur, H. S. Preparation and characterization of chitosan/poly(vinyl alcohol) chemically crosslinked blends for biomedical applications. *Carbohydr. Polym.* **76**, 472–481 (2009).
51. Sakkayawong, N., Thiravetyan, P. & Nakbanpote, W. Adsorption mechanism of synthetic reactive dye wastewater by chitosan. *J. Colloid Interface Sci.* **286**, 36–42 (2005).
52. Maciel, V. B. V., Yoshida, C. M. P. & Franco, T. T. Chitosan/pectin polyelectrolyte complex as a pH indicator. *Carbohydr. Polym.* **132**, 537–545 (2015).

Acknowledgements

This work was supported by the National Key Research and Development Project of China (2022YFE0115400), Science and Technology Research Project of Jiangxi Provincial Department of Education (GJJ2402106), and Fundamental Research Funds for the Central Universities (DUT24YG208).

Author contributions

W.Z. and C.W. supervised the project and conceived overall plan and idea. X.Y. and J.H. performed experiments, analyzed the data and prepared the figures, wrote the main manuscript text. W.Z. and C.W. carried some proof-read. All authors reviewed the manuscript.

Declarations

Competing interests

The authors declare no competing interests.

Additional information

Correspondence and requests for materials should be addressed to W.Z.